Journal of
Intelligent Material
Systems and Structures

Article

Journal of Intelligent Material Systems and Structures
23(4) 397–413

DOI: 10.1177/1045389X11434171
jim.sagepub.com
SAGE

Damage assessment of CFRP composites using a time–frequency approach

Yingtao Liu[1], Masoud Yekani Fard[1], Aditi Chattopadhyay[1] and Derek Doyle[2]

Abstract

A damage assessment methodology using a time–frequency signal processing technique is presented in this article. Delaminations are detected in composite structures with multiple stiffeners. Because Lamb waves are complex in nature, due to wave dispersion and scattering, a robust signal processing technique is required to extract features from Lamb wave signals. In this article, the matching pursuit decomposition algorithm is used for extracting wavelets from the Lamb wave signals in the time–frequency domain. A small time–frequency atom dictionary is defined to avoid the exhaustive search over the time–frequency domain and to reduce the computation costs. The propagation characteristics of Lamb waves in stiffened composite panels are investigated. The delaminations are detected by identifying the converted Lamb wave modes introduced by the structural imperfection. A two-step damage detection approach, which uses both pulse-echo and pitch-catch active sensing schemes, is developed for the identification of delaminations. The delamination is quantified using a signal energy-based damage index. The matching pursuit decomposition algorithm is further used to localize the delamination position by solving a set of nonlinear equations. The results show that the matching pursuit decomposition algorithm can be used to identify and localize the seeded delaminations in composite structures with complex geometries and material properties.

Keywords

delamination, localization, quantification, matching pursuit decomposition

Introduction

Interest in structural health monitoring (SHM) techniques and damage prognosis (DP) has increased significantly over the last few years. Well-developed DP and SHM systems inform the users about the presence of incipient damage and provide estimation of the remaining useful life (RUL) of the structures (Farrar and Lieven, 2007; Liu et al., 2010; Mohanty et al., 2010). The ultimate goal is to shift from schedule-based inspection to condition-based maintenance (CBM), which can cut down the maintenance time and reduce cost and labor requirements. Most importantly, successful implementation of these methodologies will increase the confidence levels in operating the systems and improve user safety. However, the applications of SHM are no longer restricted to terrestrial architectures. There is growing interest in the utility of SHM for space systems. The sensing methodology described in this article could also be implemented on satellite components during the assembly, integration, and test (AI&T) phase or while on-orbit to track damage and provide real-time characterization to technicians.

Although composite materials have been widely used as primary structural components in many industries, such as automotive, marine, and aerospace engineering, the characterization, detection, and quantification of multiscale damage in these heterogeneous material systems remain critical research areas. Significant research efforts have been devoted to these problems in the last few decades. Among various technologies under investigation, one of the most popular approaches for damage detection in composites is guided wave (GW)–based SHM techniques. These techniques involve exciting the structures with high-frequency elastic waves and processing the different sensing responses to detect and

[1]School for Engineering of Matter, Transport and Energy, Arizona State University, Tempe, USA
[2]Air Force Research Laboratory/Space Vehicles Directorate, Kirtland AFB, USA

Corresponding author:
Yingtao Liu, School for Engineering of Matter, Transport and Energy, Arizona State University, Tempe, AZ 85287, USA.
Email: yingtao.liu@asu.edu

characterize damage within structures. When stress waves are forced to follow a path by the material boundaries, such as for thin plates and beams, the GW is usually specified as a Lamb wave. Since aerospace and ground vehicles are fundamentally composed of simple beam, plate, and shell structures, Lamb wave–based techniques are applicable in developing SHM framework for such systems. Surface-bonded/embedded piezoelectric wafer transducers are typically used as sensors and actuators (Raghavan and Cesnik, 2007; Zhao et al., 2007). More details into the propagation of the Lamb waves can be found in previous studies (Giurgiutiu, 2005; Kessler et al., 2002; Kim and Sohn, 2007; Liu et al., 2009; Su et al., 2006). Compared to traditional SHM approaches using strain gages or fiber Bragg gratings (FBGs), the advantage of Lamb wave is that an actuator–sensor pair has a large coverage area, so that the density of sensors and actuators can be low. This advantage allows the Lamb wave–based SHM techniques to be used for monitoring large-scale structures.

Most previous research using Lamb wave–based damage detection approaches focused on simple composite structures, such as plates and beams. Fasel and Todd (2010) used ultrasonic chaotic excitations to detect various damage conditions of the composite bonded joint. A statistical classification algorithm was used to correlate the real damage state with the classification results. Lu et al. (2009) studied the mechanism of Lamb wave propagation in a stiffened panel in the time domain. Correlation analysis techniques were used for the damage identification and location. Banerjee et al. (2007) used low-frequency modal vibrations to detect impact damage and used high-frequency passive Lamb wave sensing modes to localize the damage. Lamb wave sensing signals are also complex in nature. More than one mode can be generated in a Lamb wave at any excitation frequency, and each mode has a unique dispersion curve. Most of the aforementioned work did not study Lamb wave propagation characteristics in stiffened composite panels with complex geometries. The mechanism of mode decomposition and mode conversion due to geometric discontinuities and material imperfection is still not fully understood. It is important to develop efficient analysis techniques to study the Lamb wave signals, isolate different Lamb wave modes, and extract useful information for damage detection, identification, localization, and RUL estimations in composite structures.

Damage localization in composite structures requires accurate GW information and features. Most previous work focused on locating impact damage in composite structures using passive sensing approaches (Hiche et al., 2011; Meo et al., 2005; Staszewski et al., 2009). A traditional damage localization method is to use the triangulation method and the time-of-flight (ToF) information to obtain three ellipses requiring at least three active sensors. The intersection point of the three ellipses is considered to be the damage spot. Knowledge of the group velocities of the GW in all directions is required for this approach (Coverley and Staszewski, 2003; Reynolds et al., 2009). Neural network algorithms have been used to obtain the angle-dependent group velocity profile (Moll et al., 2010). Other damage localization approaches include an analysis of direct wave paths between an actuator and multiple sensors (Sohn et al., 2005), the energy decay model (Wang and Yuan, 2006), principle stress directions for impact locations (Salamone et al., 2011), smart sensors, and sensing techniques, such as laser Doppler vibrometer (LDV; Staszewski et al., 2009) and FBG sensors (Adewuyi and Wu, 2010; Hiche et al., 2010). These approaches have been validated using isotropic and quasi-isotropic plates with simple geometries. However, limited work has addressed the extension of damage localization to general anisotropic composite structures with complex geometries.

Signal processing is necessary for extracting the features for damage detection and localization in composite structures. The goal of signal processing is not only to extract information from the sensing signal for damage detection but also to provide useful features for the damage characterization and quantification, which is important for the damage state awareness and prognosis. The traditional Fourier transform method provides the "global" information about the frequency and is suitable for signals with stationary frequency content. However, the frequency content of a Lamb wave signal varies in the time domain. This type of signal can be better represented in the time–frequency domain to extract time-varying frequency information. To analyze the time-varying sensor response effectively, the time and frequency domain characteristics must be considered simultaneously. These time–frequency representations (TFRs) characterize a given signal over the time–frequency plane by combining the time and frequency domain data. This yields more revealing information about the temporal localization of a signal's spectral components. The matching pursuit decomposition (MPD) is a time–frequency–based technique that decomposes a signal into highly localized time–frequency atoms and can provide a highly concentrated TFR (Mallat and Zhang, 1993). It is an iterative algorithm that decomposes any signal into a linear expansion of waveforms that belong to a redundant dictionary. The MPD dictionary consists of a collection of time–frequency atoms that are the dilated (time-scaled), translated (time-shifted), and modulated (frequency-shifted) versions of a single basic atom. The basic atom is often chosen to be a Gaussian signal because Gaussian signals are the most concentrated signals in both time and frequency. The MPD method has been applied to the SHM for both metal and composite structures. Das et al. (2009) developed a Monte Carlo MPD method for damage quantification in simple composite structures. But the proposed algorithm was only validated by detecting and localizing damages in

12-inch long composite beams. Chakraborty et al. (2009) used a MPD algorithm to classify the fastener failure damage in aluminum plates. An application applying the MPD method to the damage detection and feature extraction of a complex composite structure is still needed for aerospace platforms.

In this article, the MPD algorithm is first used to detect delaminations in complex composite structures. Compared to previous approaches, the proposed method significantly reduced computation cost by defining a small time–frequency dictionary. Experiments were conducted using composite panels with two stiffeners. The Lamb wave propagation in the composite panels is characterized. The group velocities of S_0 and A_0 Lamb wave modes and the angular dependence of the S_0 mode's group velocity are evaluated. Wave attenuation, particularly the S_0 mode, in terms of propagation distance is investigated. The influence of both the stiffeners and delaminations on the Lamb wave propagation is studied. A two-step damage identification approach using both pulse-echo and pitch-catch active sensing schemes is investigated in this article. The pulse-echo scheme is used for the quick global damage identification. The pitch-catch scheme provides the detailed information for the local damage identification analysis. A new signal energy-based damage index is proposed in this article. Using the proposed damage index, multiple delaminations in the composite panel can be detected and quantified.

The MPD algorithm is further used to assess the delamination location in composite structures. The sensor locations and differences of ToF were used to create three nonlinear equations. The nonlinear equations were converted into an unconstrained optimization problem and solved using Newton's method. Due to the redundancy of the PZT sensor array, a probabilistic location estimation algorithm was used to provide the confidence range of the delamination in the composite structures. Experiments were conducted using the composite structures with three types of layups and two types of carbon fiber fabrics. The localization method does not require any information about the material properties, layup, or thickness information. A confidence range for the estimated delamination is provided using the proposed methodology.

TFR of Lamb wave signal

Lamb wave propagation is complicated by wave dispersion, boundary reflections, and mode conversions. To accurately identify each Lamb wave mode and extract information to localize delamination, an advanced time–frequency analysis method is required. The MPD algorithm is used as the time–frequency analysis method to calculate the difference of ToF between sensors in this article.

For Lamb waves, the signal with finite energy, s(t), can be decomposed into a linear combination of time–frequency atoms. This type of infinite approximations can be written as

$$s(t) = \sum_{i=0}^{\infty} \beta_i g_i(t) \tag{1}$$

where $g_i(t)$ is the time–frequency atom (subwaveform) selected from the MPD dictionary A, and β_i is the corresponding expansion coefficient. The finite linear combination of these time–frequency atoms can be used to provide an approximation of the signal with high accuracy. After N iterations, the resulting expansion can be expressed as

$$s_N(t) = \sum_{i=0}^{N} \beta_i g_i(t) \tag{2}$$

The residual signal $Rs_N(t)$ with N iterations is

$$Rs_N(t) = s(t) - s_N(t) = s(t) - \sum_{i=1}^{N} \beta_i g_i(t) \tag{3}$$

Because the signal has finite energy, the energy of the approximated signal is also preserved. The energy conservation can be expressed as

$$\|s(t)\|^2 = \sum_{i=0}^{N} \|s_N(t)\|^2 + \|Rs_N(t)\|^2 \tag{4}$$

In order to find the best match between the signal and time–frequency atoms, the inner product of the signal and each time–frequency atom is calculated. Let $g(t) \in A$, where the signal, s(t), can be decomposed into wavelets as shown by

$$s(t) = \langle s(t), g(t) \rangle g(t) + Rs \tag{5}$$

where Rs is the residual signal after approximation using the time–frequency atom, g(t). To minimize the energy of Rs, the proper g(t) is defined to satisfy the equation

$$|\langle s(t), g(t) \rangle| \geq \beta \sup |\langle s(t), g(t) \rangle| \tag{6}$$

where β is an optimality factor that satisfies $0 < \beta \leqslant 1$, and $\sup|\langle s(t), g(t) \rangle|$ is the least upper bound of the inner product of $\langle s(t), g(t) \rangle$. The decomposition of signal s(t) is completed by successive calculation with time–frequency atoms from the dictionary. Let $g_i(t)$ be the time–frequency atom of the ith iteration, and the approximated signal at this iteration is

$$s_i(t) = \langle Rs_i(t), g_i(t) \rangle \tag{7}$$

when $i = 0$, let $Rs_0 = e(t)$. According to equations (2), (5), and (7), the approximated signal with a total of N iterations is

$$s_N(t) = \sum_{i=1}^{N} \langle Rs_i(t), g_i(t) \rangle \quad (8)$$

and the original signal can be expressed as

$$s(t) = \sum_{i=1}^{N} \langle Rs_i(t), g_i(t) \rangle + Rs_N \quad (9)$$

where Rs_N is the residual signal at the Nth iteration. Although a redundant dictionary can provide flexible decomposition of the signal, the computational cost is consequentially high. To reduce the number of unnecessary time–frequency atoms, a modified MPD algorithm is used. The time–frequency dictionary of the MPD algorithm is optimized based on the features of the Lamb wave signals from the structures being interrogated. Limited subwaveforms that can best represent the original signal are included in the dictionary. By using the optimized atom dictionary, the original signal can still be efficiently decomposed with high local time–frequency resolution.

The actuation signal used in the experiments conducted here is a cosine burst wave. According to the Lamb wave theory, only S_0, A_0, and the related converted modes exist as subwaveforms. These subwaveforms can be expressed as

$$s(t) = e^{-\beta t^2} \cos(2\pi f t) \quad (10)$$

where the constant β defines the width of the burst wave and f is the central frequency. S_0, A_0, and the related converted modes can be obtained by the dilation and translation of the basic subwaveform. This procedure reduces the size of the MPD dictionary significantly. It must be noted that the MPD algorithm efficiently yields a compact representation of the burst wave signals in terms of selected basic atoms in the dictionary. Therefore, it reduces the computational cost significantly. In addition, the noise is filtered out because the noise waveforms are typically orthogonal to the selected atoms.

Using the refined MPD algorithm, the GW signals from different sensors can be represented in the same time–frequency domain. The difference of ToFs between sensors can be compared and accurately calculated. This ToF information is used as input information for the damage location objective equations.

Wave characterization in a composite panel

Damage identification using Lamb wave propagation approaches requires an in-depth understanding of the properties of the various types of wave modes transmitting in the structures with or without damage. In thin-walled structures, such as plates, beams, and shells, Lamb waves can propagate a relatively large distance. A few sensors can cover a large area using the Lamb wave analysis approach. This is generally true for isotropic materials and homogeneous structures. The process is more complex in composite structures. The complex geometry and material properties of the composite panels can cause signal scattering and other energy dissipation effects. The basic Lamb wave characteristics, such as the group velocities of S_0 and A_0 modes and the angular group velocities, need to be calculated as a function of angle relative to composite orientation. More detailed Lamb wave propagation and mode conversions can be detected when the basic Lamb wave characteristics have been evaluated.

Experimental setup

Four carbon fiber polymer matrix composite panels with $(0°/90°/0°)_s$ layup were fabricated in-house. Each panel has two cocured blade stiffeners on its surface, as shown in Figure 1. Plain weave carbon fiber fabrics were used as the fiber reinforcement. The epoxy FS-A23 (resin) and FS-B412 (hardener; Epoxy System Inc.) were used as the matrix system. A total of nine PZT wafers and one PZT ring were surface bonded on the stiffened side of the panel surface. The dimensions of the structure and the locations of the PZTs are shown in Figure 2. Two composite panels were

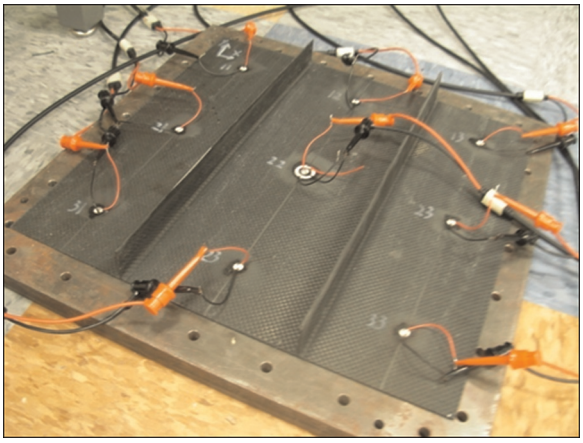

Figure 1. Stiffened composite panel with bonded PZT patches.

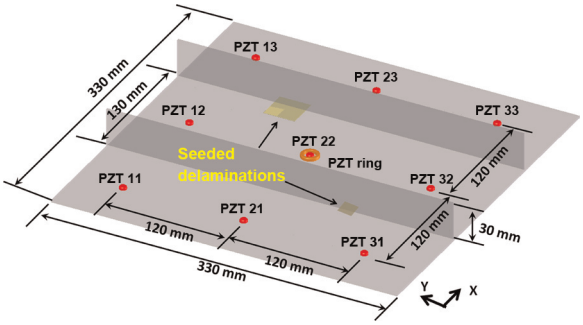

Figure 2. Dimensions of the composite panel and PZT patches.

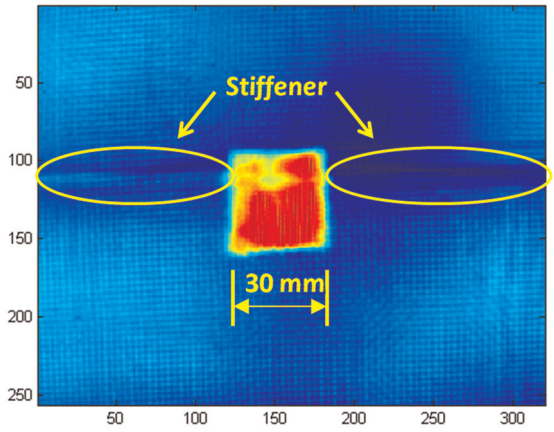

Figure 3. Flash thermography image of composite stiffened panel with 30 × 30-mm^2 delamination.

fabricated with seeded delaminations. Two Teflon patches were inserted during layup to generate delaminations. The other two composite panels were fabricated without delaminations to study the healthy state of the composite panels. A flash thermography (model: EchoTherm; Thermal Wave Imaging, Inc. Ferndale, Michigan.) system was used to visualize the delaminations as shown in Figure 3. A waveform was generated using the NI 5412 waveform generator, and the Lamb wave signals were captured using the NI 5105 digitizer at the sampling frequency of 20 MHz. In order to optimize the central frequency of the actuation signal, several actuation signals were generated using central frequencies varying from 10 to 300 kHz in 10-kHz increments. Ten observations were recorded at each frequency, and the sensor signal was averaged from these observations to reduce the sampling error.

Group velocity calculation and wave attenuation analysis. Most Lamb wave approaches, such as mode decomposition and the ToF calculation, require the group velocity of each Lamb wave mode. Group velocities of S_0 and A_0 Lamb wave modes are the most basic parameters used in the Lamb wave analysis. Theoretically, the group velocity at any frequency can be calculated and illustrated using dispersion curves. However, due to the material complexity, group velocities of S_0 and A_0 modes are calculated using experimental data in this article. PZT 22 was used as the actuator, and PZTs 12 and 32 were used as the sensors. The signal recorded from PZT 12 is shown in Figure 4(a). Due to the size limitation of the sample, the first two Lamb wave packages (S_0 mode and the S_0 reflection mode) overlap in the time domain. It is difficult to calculate the ToF of the S_0 mode because the center of S_0 mode cannot be localized. However, the TFR of the sensor signal clearly represents the first three Lamb wave packages in the time–frequency domain, as shown in Figure 4(b).

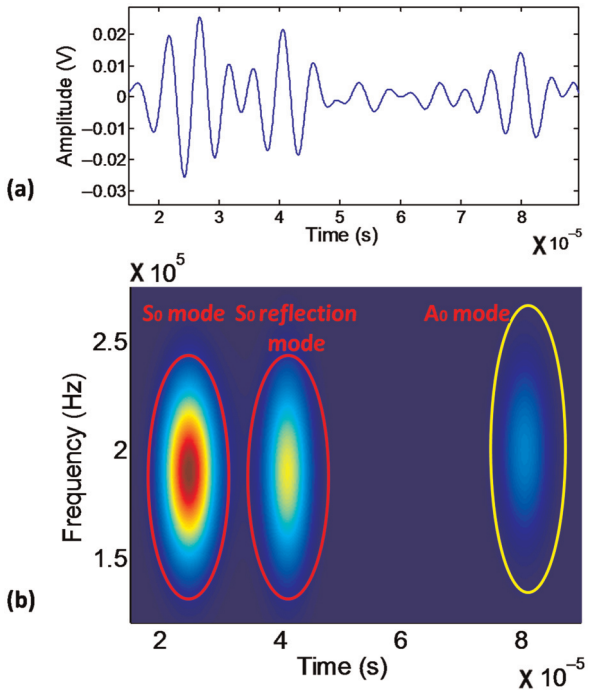

Figure 4. (a) Signal of the Lamb wave recorded from PZT 12 and (b) TFR of the Lamb wave recorded from PZT 12.

Because the propagation distances are known, these three Lamb wave packages can be identified as the S_0 mode, S_0 reflection mode from the boundary, and the A_0 mode. Similar results can be obtained by studying the data recorded from PZT 32. Therefore, the group velocities of S_0 and A_0 modes can be accurately calculated as 5250 and 1470 m/s, respectively.

The angular dependence of Lamb wave propagation is studied by comparing the velocities of the S_0 mode along all the possible actuator–sensor paths. When PZT 11 was used as the actuator, five possible paths are between the 0° and 90° range. It is noted that since the composite panel was fabricated using plain weave fiber fabric, and the fiber fabric structure in the 0° and 90° is the same, the velocity of S_0 at 0° and 90° is the same. The S_0 mode's group velocity at each detectable angle is shown in Figure 5. It is observed that at 0°, the S_0 mode has the highest propagating velocity (5.25 m/ms). At 45°, the S_0 mode has the lowest propagating velocity (4.01 m/ms). The S_0 mode's group velocity at different angles is used to identify the arrival and reflection of the S_0 mode in the Lamb wave decomposition for damage identification in the following section.

Lamb wave attenuation

Wave attenuation is defined as the reduction of signal amplitude with the propagation distance. It is a critical feature for the effectiveness of damage detection using Lamb wave techniques. The attenuation rate of a Lamb

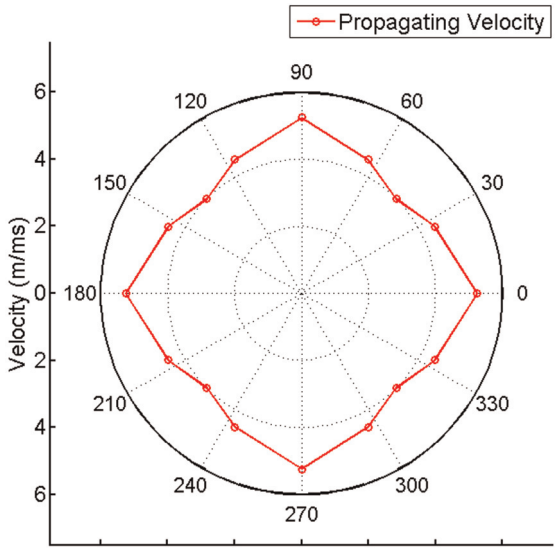

Figure 5. Angular dependence of wave propagating velocity (S_0 mode) in the composite panel.

wave signal is a function of the wave frequency and the propagation distance, which can be expressed as equation (11)

$$A \sim F(f, d) \tag{11}$$

where A is the attenuation rate of individual Lamb wave signal with a frequency f and a propagation distance d, respectively.

Lamb wave attenuation is studied using the composite panels with seeded delaminations. PZT 22 was used as the actuator. Lamb wave signals collected from PZTs 12 and 21 are analyzed to study the influence of the blade stiffener on the propagation of Lamb waves. The first received S_0 mode can be easily isolated from the other Lamb wave modes because it has the highest group velocity. Therefore, the first measured S_0 mode can be used to determine the wave attenuation. More severe wave attenuation is observed when Lamb waves propagate through stiffeners, as shown in Figure 6. The horizontal axis represents the ToF of the first arrived S_0 mode from the actuator to the sensor. The amplitude plotted on the vertical axis demonstrates the reduction of wave amplitude. It is observed that the amplitude of the S_0 mode collected from PZT 21 is 57% of that recorded from PZT 12. The results indicate that the presence of stiffeners significantly reduces the energy of the Lamb wave. The signals collected from PZTs 31 and 13 are used to study the influence of the delamination sizes on the propagation of Lamb waves. As shown in Figure 7, the amplitude of the S_0 mode reduced more severely when it propagated through a larger delamination area. It is observed that the amplitude of the S_0 mode collected from PZT 31 is 55% of that recorded from PZT 13. The delamination size has a significant influence on the Lamb wave attenuation.

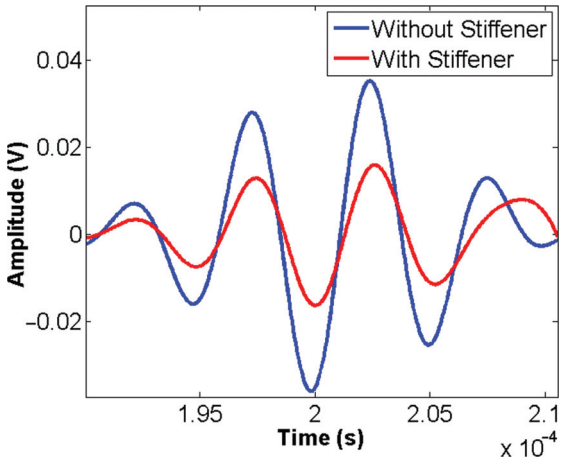

Figure 6. Wave attenuation of the S_0 mode from PZTs 12 and 21.

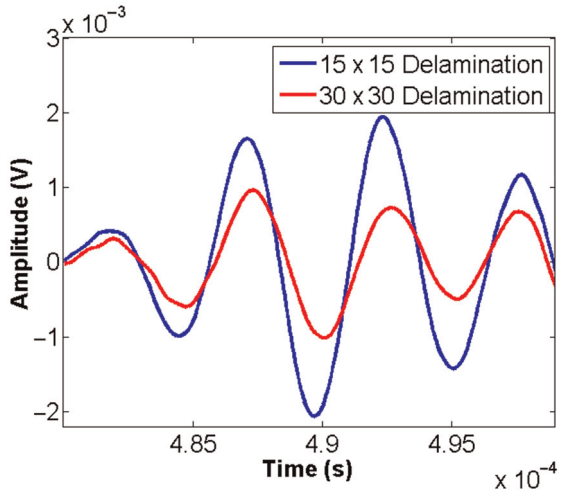

Figure 7. Wave attenuation of the S_0 mode from PZTs 13 and 31.

The wave amplitude represents the signal energy at a specific instant. The reduction of signal energy can be used to illustrate the wave attenuation for the whole signal. The signal energy can be expressed as

$$E(s) = s^2(t)dt \tag{12}$$

where E(s) is the energy of signal s(t). By calculating the energy of signals recorded from each PZT sensor, the influence of the stiffener and delamination can be clearly illustrated. When PZT 22 was used as the actuator, the signal energy was normalized by the largest sensor signal. It is observed that signal from PZT 32 has the largest energy, so the normalized signal energy of PZT32 is 1. The other signal energies are calculated accordingly. Figure 8 shows the normalized signal energy collected from all the PZT sensors. Since there is no stiffener or delamination between the actuator and PZTs 12 and 32, the signals recorded from the two PZTs have similar amount of energy. The stiffeners

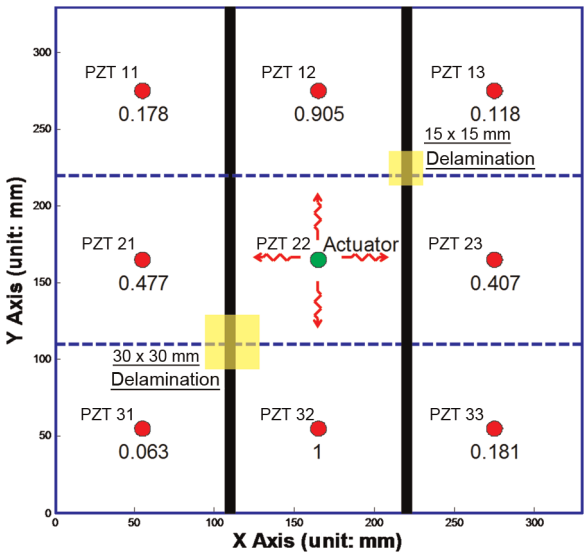

Figure 8. Normalized PZT sensor signal energy.

most significantly influence the signals recorded from PZTs 21 and 23. The signals recorded from PZTs 11 and 33 were also influenced only by the stiffeners. However, due to the longer propagation distances and the angel between fiber orientation and wave propagation direction, the signals from PZTs 11 and 33 showed more energy loss than PZTs 21 and 23. For PZTs 31 and 13, both the stiffeners and delamination caused the severe energy loss. A larger energy loss from PZT 31 correlates with a larger delamination size.

Damage detection using the time–frequency analysis

Global and local damage identification framework

The general purpose of damage detection using active sensing in SHM is to find the change of sensing features before and after structural degradation. Robust damage features can represent the damage initiation and monitor the DPs. In this article, a damage detection methodology is proposed by using the MPD algorithm and the pulse-echo and pitch-catch active sensing schemes. The MPD algorithm represents the PZT sensing signals in the time–frequency domain. Additional converted Lamb wave modes of the sensor signals can be identified in the TFR when delaminations exist in the composite structures and are used as the sensing features. The advantages of MPD algorithm include (a) remove the signal noise; (b) extraction of robust Lamb wave modes, and (c) high resolution in both time and frequency domains. A two-step damage detection methodology using the pulse-echo and pitch-catch schemes can identify the existence of delamination damage as well as provide location information. Using only one sensor and one actuator, pulse-echo approach can quickly detect the existence of damage in a large composite structure. A single PZT ring sensor is sufficient to interrogate the entire composite panel. The pulse-echo scheme can provide quick damage estimation at the global level. Once the delamination is detected, the pitch-catch approach will provide detailed information of damage location and severity using a PZT array with eight PZT wafer sensors. The detailed local detection information can be used for future prognosis and RUL estimation.

The concept of the two-step global and local damage detection strategy can be applied to the SHM of large engineering structures such as aircraft wings and fuselages. Global detection can examine the structural integrity in a short time. Once potential structural damage is detected, local damage detection can identify the detailed location, severity, and damage type for further maintenance.

Global damage detection using a pulse-echo scheme

A pulse-echo scheme is first used to detect the existence of delamination. The composite panel's complex geometry introduces several reflection modes to the sensor signal when the pulse-echo scheme is used for damage detection. To successfully detect delamination, the different reflection modes need to be isolated and identified. When the S_0 mode arrives at the T-section of the blade stiffener, the mode scatters into three components: one propagating in the plate, one propagating in the blade stiffener, and a reflection in the plate, as shown in Figure 9(a). Similarly, when the component of the S_0 mode that is transferred into the blade stiffener reflects back to the T-section, this mode also scatters into another three components. Two of these propagate along different directions in the plate and the third is reflected back into the stiffener, as shown in Figure 9(b).

Due to the Lamb wave scattering at the T-section, the S_0 and A_0 modes generated by the actuator propagate along different possible paths and finally are recorded by the PZT ring sensor. The eight shortest possible Lamb wave propagation paths are shown in Figure 9(c). Both the propagation distance and the group velocities of S_0 and A_0 modes are known; therefore, the theoretical ToF along each propagation path can be calculated, as shown in Tables 1 and 2. Since PZT 22 is placed in the center of the panel, path 6 is the same in both the X and Y directions. Therefore, path 6 will contain Lamb waves from both the X and Y directions, which results in an increase in magnitude.

In Figure 10, the S_0 mode conversion is considered when an S_0 wave mode arrives at the stiffener. Mode conversion occurs at the T-section because of the thickness change. The original S_0 mode converts into A_0 and S_0 modes and propagate along the three possible directions. Due to the low group velocity of the A_0 mode,

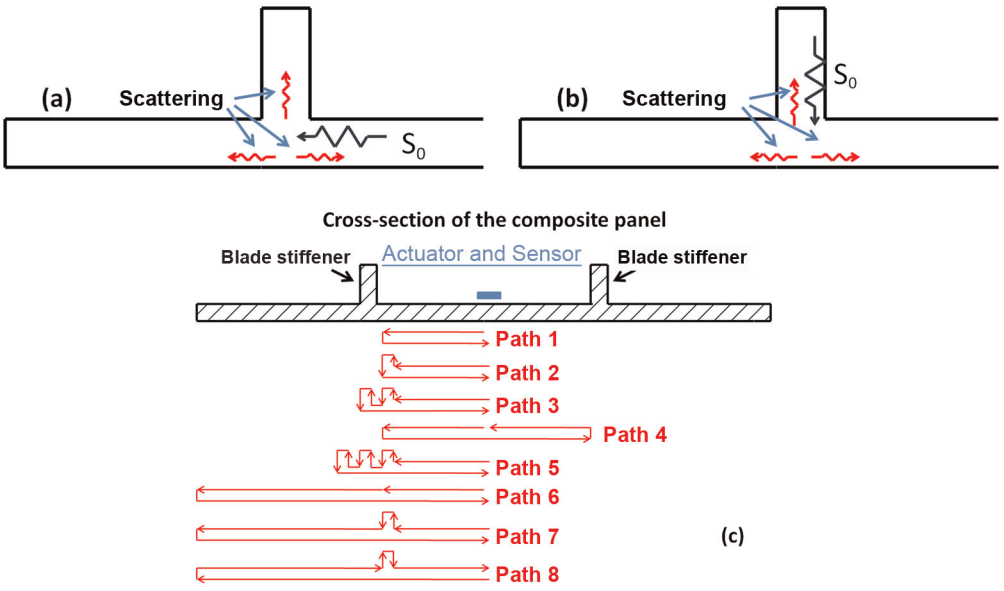

Figure 9. (a) Lamb wave mode scattering into T-section; (b) Lamb wave mode scattering from T-section; and (c) different paths of Lamb wave propagation in the stiffened composite panel using the pulse-echo approach.

Table 1. ToF analysis for the S_0 mode.

	Path distance (m)	Group velocity of S0 mode (m/ms)	Time of flight (ms)
Path 1	0.13	5.25	0.0248
Path 2	0.19	5.25	0.0362
Path 3	0.25	5.25	0.0476
Path 4	0.26	5.25	0.0495
Path 5	0.32	5.25	0.0610
Path 6	0.33	5.25	0.0629
Path 7	0.39	5.25	0.0743
Path 8	0.39	5.25	0.0743

ToF: Time of flight.

Table 2. ToF analysis for the A_0 mode.

	Path distance (m)	Group velocity of S0 mode (m/ms)	Time of flight (ms)
Path 1	0.13	1.47	0.0884
Path 2	0.19	1.47	0.1292
Path 3	0.25	1.47	0.1700
Path 4	0.26	1.47	0.1768
Path 5	0.32	1.47	0.2176
Path 6	0.33	1.47	0.2240
Path 7	0.39	1.47	0.2653
Path 8	0.39	1.47	0.2653

ToF: Time of flight.

only the converted A_0 mode reflected back to the PZT ring sensor was recorded in the experiment. However, the reflected converted A_0 mode cannot be clearly displayed in the TFR because of the low energy caused by wave scattering and attenuation.

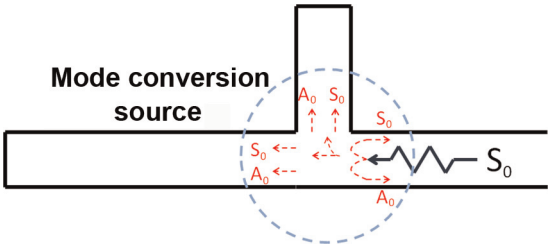

Figure 10. Mode conversion at T-section.

The healthy composite panel is used to identify each Lamb wave mode for the echo signal. A burst wave with a central frequency of 180 kHz was used to generate the Lamb wave. The Lamb wave echo signal was recorded from the PZT ring sensor. The TFR of the echo signal is shown in Figure 11. The first two atoms can be easily identified as the S_0 mode propagates along paths 1 and 2, respectively. The experimental ToF of the two atoms matches with the theoretical calculation. Since paths 3 and 4 have close path lengths, the S_0 modes propagating along the two paths overlap together in the time–frequency domain and represent as the third atom in Figure 11. Similarly, the S_0 modes propagating along paths 5 and 6 merge and are seen as the fourth atom in Figure 11. The fifth atom is identified as the A_0 mode since the experimental ToF of this mode matches with theoretical calculation shown in Table 2. The theoretical and experimental results for ToF are compared in Table 3. Due to the signal attenuation and multiple reflections and scatterings, it is noted that the S_0 mode propagating along paths 7 and 8 lose most of the signal energy. There is no clear TFR for this mode in the time–frequency domain. It

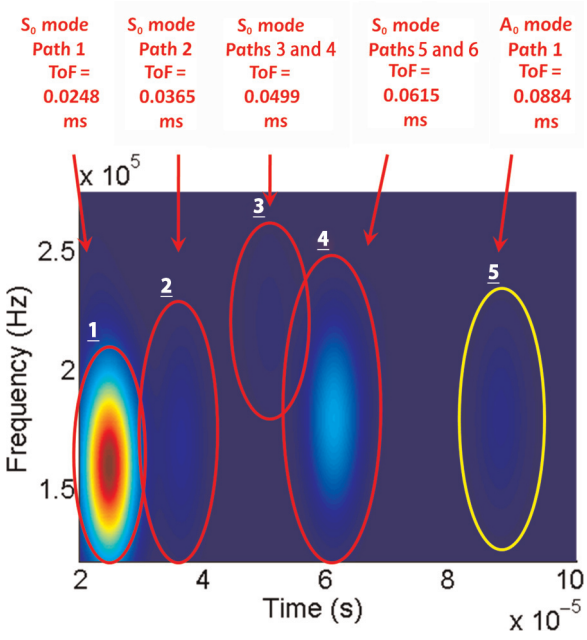

Figure 11. TFR and the mode identification of the echo Lamb wave using the healthy stiffened panel.

Table 3. ToF comparison for the S_0 modes.

	Theoretical time of flight (ms)	Measured time of flight (ms)
Path 1	0.0248	0.0248
Path 2	0.0362	0.0365
Path 3	0.0476	0.0499
Path 4	0.0495	0.0499
Path 5	0.0610	0.0615
Path 6	0.0629	0.0615

ToF: Time of flight.

can be reasonably concluded that the S_0 mode, which propagates longer than paths 7 and 8, can be ignored.

Delamination was detected in the damaged composite stiffened panel. Using the MPD time–frequency analysis algorithm, the TFR of the echo signal can be demonstrated, as shown in Figure 12. Compared to the TFR shown in Figure 11, the S_0 mode propagating along paths 1–6 and the A_0 mode can be identified at the same time instance. In addition, one more atom is detected in this TFR. When the S_0 modes propagate through the delamination of the composite panel, the two modes convert into a new mode, which can be named as the MC mode. In fact, there are several MC modes due to multiple delaminations. After several reflections of the stiffeners and boundaries, the MC modes overlap and combine with each other. This combined MC mode is recorded by the PZT ring sensor. The new atom correlates with the delaminations in the composite panel. Using the global pulse-echo scheme,

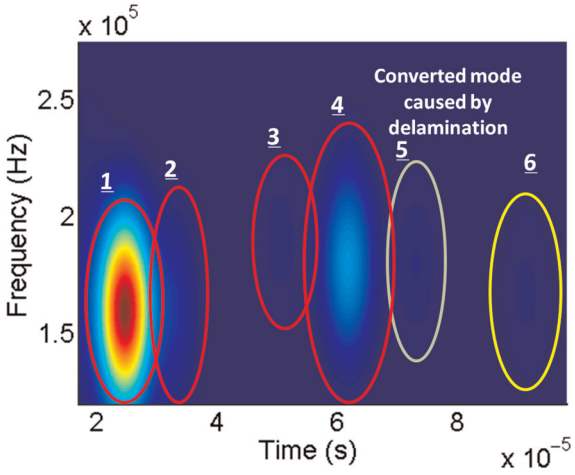

Figure 12. TFR and the mode identification of the echo Lamb wave using the stiffened panel with delamination.

the delaminations can be quickly detected by one single PZT ring sensor. However, the pulse-echo approach cannot provide more information about the location, number of delaminations, and so on A local pitch-catch active sensing scheme is necessary to obtain these details.

Local damage detection using a pitch-catch scheme

Once delamination is detected using the global scheme, local damage detection approach is used to find more detailed damage information. The pitch-catch scheme uses a sensor array with nine PZT wafers to detect the local delamination between the actuator and sensors. PZT 22, which is located at the center of the composite panel, is used as the actuator. A burst signal with a central frequency of 180 kHz is used as the excitation signal. The PZT sensor signal recorded from the healthy panel is used as the baseline data. The first five Lamb wave atoms in the TFR are identified using the baseline data. Delamination is detected by identifying the new MC modes in the signal recorded from the panel with delaminations, which is similar to the pulse-echo approach.

Using the healthy composite panel, the sensor signal collected from PZT 21 is used to study the influence of the stiffened panel on the sensor signal. The first four possible propagation paths for PZT 21 are shown in Figure 13, and the associated TFR is shown in Figure 14. The first S_0 and the following reflection of S_0 modes are illustrated. The arrival of the A_0 mode was recorded at 0.086 ms. The experimental ToF results match with the theoretical analysis. Similar time–frequency atoms with more attenuation and time shift can be identified in the signal collected from the other PZT sensors.

Two delaminations were detected between PZTs 22 and 31 and PZTs 22 and 13. The TFR of the sensor

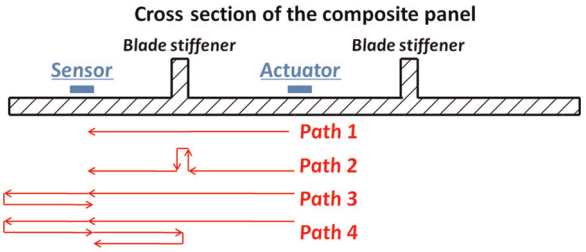

Figure 13. Possible propagation paths for PZT 21.

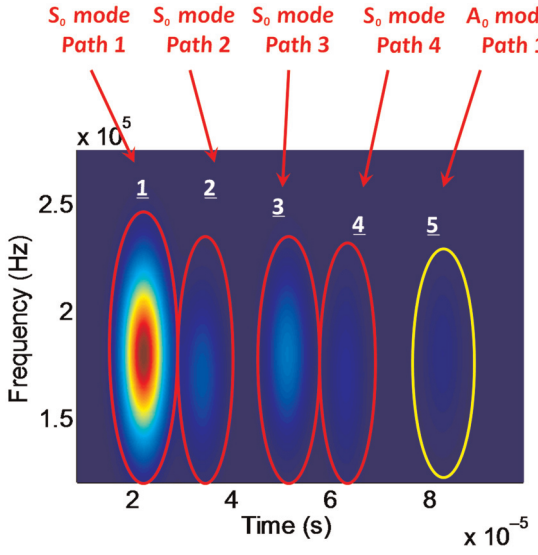

Figure 14. TFR of Lamb wave collected from PZT 21 using a healthy panel.

signal recorded from PZT 31 using the healthy panel is shown in Figure 15. Each Lamb wave mode can be represented as a time–frequency atom in the TFRs. The location of each atom in the TFR can be verified by studying the ToF of each Lamb wave mode. As shown in Figure 15, the first time–frequency atom is identified as the first arrived S_0 mode, and the second and the third atoms are the S_0 reflection modes due to the boundary and the stiffener. The fourth atom is the A_0 mode. Similar atoms can be identified in the sensor signals recorded using the composite panels with seeded delaminations. However, using the damaged composite panel, the fifth atom in the TFR of the PZT 31 signal is identified as the converted mode caused by the delamination, as shown in Figure 16. Due to the delamination between PZTs 22 and 13, the converted mode is also detected in the signal recorded from PZT 13. However, in the sensor signals of PZTs 11 and 33, there is no such converted mode introduced by delamination. These results demonstrate that the two seeded delaminations are detected by the local PZT sensor using the pitch-catch active sensing scheme. Using the proposed methodology, multiple delamination damages can be detected.

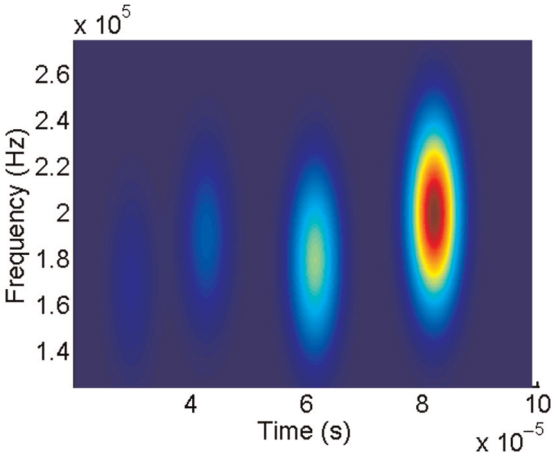

Figure 15. TFR of Lamb wave collected from PZT 31 using a healthy composite panel.

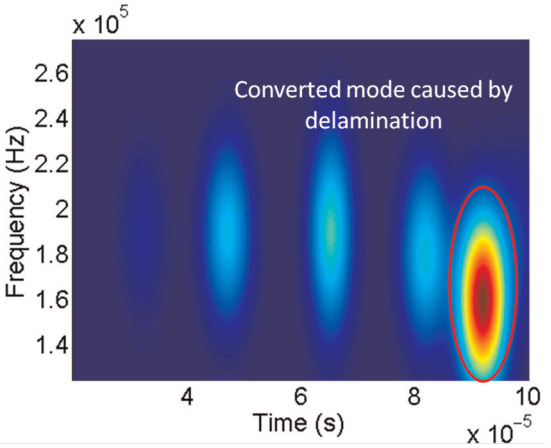

Figure 16. TFR of Lamb wave collected from PZT31 using a composite panel with delaminations.

Damage quantification using damage index. Damage indices have been proved to be useful for damage quantification in composite structures with different geometries and loading conditions (Dalton et al., 2001; Diligent et al., 2002; Ihn and Chang, 2004a, 2004b; Kim et al., 2003). By selecting appropriate Lamb wave modes from the sensor measurements, the following damage index is proposed to quantify the delamination size

$$DI = a\left(\frac{\int_{t_1}^{t_2}|s(t)|^2dt}{\int_0^T|s(t)|^2dt}\right)^k \quad (13)$$

where DI is the defined damage index, a and k are the gain factors, s(t) denotes the time-varying spectral amplitude of Lamb wave signal, t_1 and t_2 denote the start and end point of a mode, and T is the total time length of a signal. The value of a and k can be chosen

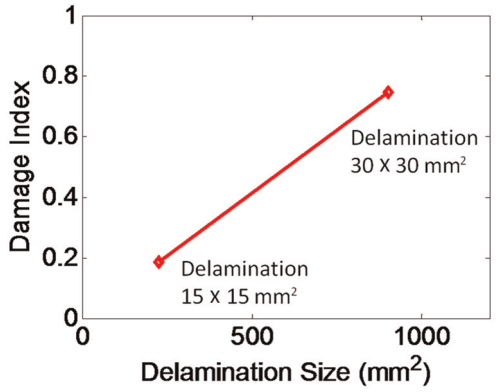

Figure 17. Quantified delamination in composite panels using proposed damage index.

empirically. In this article, a is chosen as 10,000 and k is chosen as 4.5 to obtain a linear response of delamination size. $\int_{t_1}^{t_2} |s(t)|^2 dt$ expresses the energy of a special Lamb wave mode. $\int_0^T |s(t)|^2 dt$ expresses the total signal energy. The energy of the converted mode is calculated using the MPD algorithm. During the decomposition procedure of Lamb wave signals, the energy of each mode is calculated and saved. The total energy of the signal can be obtained after the decomposition by computing the summation of mode energy. Using the defined damage index, the size of the delamination can be estimated. Typically, the greater the delamination, the larger the energy fraction of the converted mode. The calculated damage index and delamination sizes are shown in Figure 17. By choosing a and k values properly, the proposed damage index shows a good linear response to delamination size. The delaminations in the stiffened composite panels can be properly quantified.

Although the developed damage detection schemes are validated using composite structures, the method can be extended to metallic and complex engineering structures. The mode conversions and signal energy reduction of Lamb wave due to damage are also true in metallic materials. The two-step global and local damage detection schemes provide the quick damage detection option as well as the detailed damage awareness option. This is important especially for the SHM of complex engineering structures and systems. Therefore, the developed global and local detection schemes using the MPD algorithm have potential application to detect different damage scenarios.

Damage localization using the time–frequency analysis

The proposed time–frequency method using the developed MPD algorithm is extended to localize delaminations in composite structures with complex geometries. A PZT sensor array is used to detect the delamination location. The MPD algorithm is used to compute the differences of the ToF of the converted modes between master and slave sensors. To assess the delamination location in composite structures, the sensor locations and differences of ToF are used to create three nonlinear equations. The nonlinear equations are converted into an unconstrained optimization problem and solved using Newton's method. Due to the redundancy of the PZT sensor array, a probabilistic location estimation algorithm is used to provide the confidence range of the delamination in the composite structures. Experiments are conducted using the composite structures with three types of layups and two types of carbon fiber fabrics. The damage localization method does not require any information about the material properties, layup, or thickness information. A confidence range for the estimated delamination is provided using the proposed methodology.

Damage localization algorithm

The delamination localization algorithm for composites is based on the difference of ToF of the converted modes caused by delamination. A piezoelectric-based active sensing method is used to localize delamination in composites. The actuator and sensor placement is shown in Figure 18. Providing that the center of the delamination in the composite plate is (x_d, y_d) and the sensor positions are (x_i, y_i) $(i = 1, 2, \ldots, 6)$. The distance between the delamination and each PZT sensor is D_i and expressed as

$$D_i^2 = (x_d - x_i)^2 + (y_d - y_i)^2 \tag{14}$$

For this technique, a Lamb wave is first generated by the actuator. When the Lamb wave propagates through the delamination area, mode conversions and reflections can scatter the Lamb wave in all directions

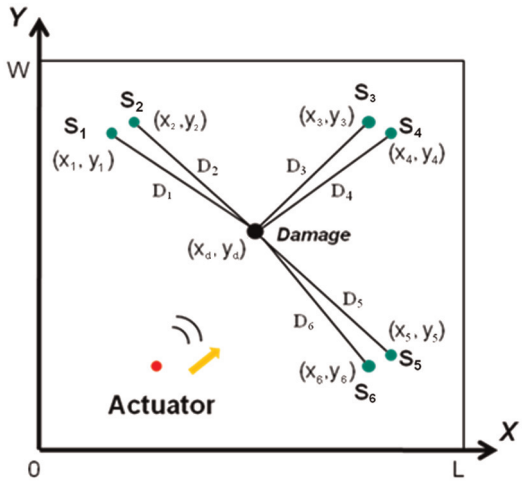

Figure 18. Actuator and sensor placement on composite samples.

in the composite. The ToF, T_i, from the delamination to the sensor, S_i, combines with the group velocity, V_i, to yield a new expression for distance

$$D_i = T_i V_i \tag{15}$$

The group velocity of a Lamb wave is a function of fiber orientation, material properties, thickness, and so on. As most composite structures are anisotropic materials, which have different material properties in different directions, the group velocity is different for each direction. In short, V_i $(i = 1, 2, \ldots, 6)$ have unique values for various directions. However, as shown in Figure 19, when two sensors S_1 and S_2 are placed close to each other but far from the delamination, we have D_1, $D_2 \gg d_{12}$.

$$\frac{d_{12}}{D_1} \approx \frac{d_{12}}{D_2} \approx \sin(\propto) \approx 0 \tag{16}$$

where d_{12} is the distance between sensors S_1 and S_2. We can assume $\propto \approx 0$. The group velocities from the delamination to the sensors can be assumed to be the same

$$V_i \approx V_{i+1} (i = 1, 3, 5) \tag{17}$$

Based on equations (14), (15) and (17), three equations with eight unknowns are present and can be consolidated to yield a generic equation for comparing the two velocities

$$\frac{\sqrt{(x_d - x_i)^2 + (y_d - y_i)^2}}{T_i} = \frac{\sqrt{(x_d - x_{i+1})^2 + (y_d - y_{i+1})^2}}{T_{i+1}} \tag{18}$$

where i can be equal to 1, 3, 5. The unknown variables are x_d, y_d, and T_i $(i = 1, 2, \ldots, 6)$ associated with delamination location and the ToF of propagated mode conversions resulting from wave interaction with the delamination. The nonlinear equations condensed in equation (18) cannot be solved because there are more unknown variables than equations. In order to provide additional information, one sensor is picked as the master sensor, and the other sensors are used as slave sensors. The differences of ToF of the converted modes between the master sensor and each slave sensors can be written as

$$T_{s,j} = T_m + \Delta T_{j,m} \tag{19}$$

where $T_{s,j}$ is the ToF of the converted mode for the slave sensor j $(j = 1, \ldots, 5)$, T_m is the ToF of the converted mode for the master sensor, and $\Delta T_{j,m}$ is the difference of ToFs between master sensor and slave sensor j. Using the time–frequency analysis approach, $\Delta T_{j,m}$ can be solved by identifying the converted modes of the Lamb wave signal in the time–frequency domain. The selection of the master sensor is random. If sensor S_1 is chosen as the master sensor, the nonlinear equation (18) can be written as

$$\begin{aligned}
&\frac{\sqrt{(x_d - x_1)^2 + (y_d - y_1)^2}}{T_1} - \frac{\sqrt{(x_d - x_2)^2 + (y_d - y_2)^2}}{T_1 + \Delta T_{2,1}} = 0 \\
&\frac{\sqrt{(x_d - x_3)^2 + (y_d - y_3)^2}}{T_1 + \Delta T_{3,1}} - \frac{\sqrt{(x_d - x_4)^2 + (y_d - y_4)^2}}{T_1 + \Delta T_{4,1}} = 0 \\
&\frac{\sqrt{(x_d - x_5)^2 + (y_d - y_5)^2}}{T_1 + \Delta T_{5,1}} - \frac{\sqrt{(x_d - x_6)^2 + (y_d - y_6)^2}}{T_1 + \Delta T_{6,1}} = 0
\end{aligned} \tag{20}$$

In equation (20), there are three unknown variables, and in these three nonlinear equations, the unknowns are x_d, y_d, and T_1. Theoretically, these equations can be solved. More Lamb wave propagation information, such as group velocities in different directions, can also be calculated after solving equation (20).

To efficiently solve the nonlinear equations, they are combined and solved using an unconstrained Newton's method. The Newton's method has been proven to be an efficient iterative method for finding roots of equations (Rao, 1996). In optimization, the Newton's method is equivalent to iteratively minimizing a local quadratic approximation to the objective function.

The localization objective equation (20) can be written as

$$\mathbf{F}(\mathbf{x}) = 0 \tag{21}$$

where $\mathbf{F}$ is the vector of the equations F_i $(i = 1, 2, 3)$ and $\mathbf{x}$ is the vector of the unknowns. For vector $\mathbf{x}$, we have

$$x_1 = x_d; x_2 = y_d; x_3 = T_1 \tag{22}$$

Assume at $\mathbf{x}^*$, we have $\mathbf{F}(\mathbf{x}^*) = 0$. The Newton's method converges to $\mathbf{x}^*$ by computing the Jacobian matrix of the function $\mathbf{F}$. The Newton's iteration can be expressed as

$$\mathbf{x}^{n+1} = \mathbf{x}^n + \delta\mathbf{x}^n = \mathbf{x}^n - \mathbf{J}(\mathbf{x}^n)^{-1}\mathbf{F}(\mathbf{x}^n) \tag{23}$$

where $\mathbf{x}^n$ is the current point, $\mathbf{x}^{n+1}$ is the iteration point after $\mathbf{x}^n$, and $\delta\mathbf{x}^n = \mathbf{J}(\mathbf{x}^n)^{-1}\mathbf{F}(\mathbf{x}^n)$. The Jacobian matrix $\mathbf{J}(\mathbf{x})$ can be expressed as

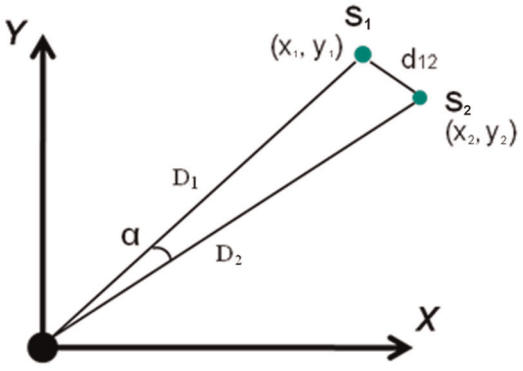

Figure 19. Scheme of optimized sensor arrangement.

$$\mathbf{J}(\mathbf{x}) = \frac{\partial \mathbf{F}(\mathbf{x})}{\partial \mathbf{x}} = \begin{bmatrix} \frac{\partial F_1(x)}{\partial x_1} & \frac{\partial F_1(x)}{\partial x_2} & \frac{\partial F_1(x)}{\partial x_3} \\ \frac{\partial F_2(x)}{\partial x_1} & \frac{\partial F_2(x)}{\partial x_2} & \frac{\partial F_2(x)}{\partial x_3} \\ \frac{\partial F_3(x)}{\partial x_1} & \frac{\partial F_3(x)}{\partial x_2} & \frac{\partial F_3(x)}{\partial x_3} \end{bmatrix} \quad (24)$$

For unconstrained optimization, the merit function measures the agreement between the function value and the ideal optimized value. Generally, the merit function can be written as a scalar-valued function

$$f(\mathbf{x}) = \|\mathbf{F}(\mathbf{x})\|^2 \quad (25)$$

The solution $\mathbf{x}^*$ of nonlinear equations, $\mathbf{F}(\mathbf{x}) = 0$, is also the global minimum of the objective function $f(\mathbf{x})$. The Newton's method is used in this article to find the global minimum solution for the objective function.

Assuming that the same group velocities for the two nearby PZT sensors on the composite specimen introduces system estimation error to the proposed algorithm and increases uncertainty of the estimated delamination location. Probability-based location estimation can provide a certain location range and improve the damage awareness in composite structures.

Redundant PZT sensors are used in the proposed localization method. Four pairs of sensors are bonded on each composite sample. For every composite sample, round robin experiments were conducted. Each PZT transducer was used as an actuator once in the eight experiments. Based on equation (25), eight delamination positions can be estimated. They are $(x_{d,i}, y_{d,i})$ $(i = 1, 2, \ldots, 8)$. Since a different actuator is used in each experiment, the experiments can be considered independent. The final delamination position (x_d, y_d) is defined as

$$x_d = \frac{\sum_{i=1}^{i=n} x_{d,i}}{n}, \quad y_d = \frac{\sum_{i=1}^{i=n} y_{d,i}}{n} \quad (26)$$

where (x_d, y_d) is the final estimated delamination position and n is the total amount of experiments conducted for each composite sample. For the cases studied in this article, n is equal to 8.

The delamination positions in the *x*- and *y*-axes are also independent to each other. To define the estimated data vector, **D**, the following equation can be used

$$\mathbf{D} = \{d_m\} = \left[x_{d,1}, \ldots, x_{d,8}, y_{d,1}, \ldots, y_{d,8}\right] \quad (27)$$

The confidence range of the delamination can be estimated by calculating the standard deviation, α, of vector **D** (Papoulis and Pillai, 2002)

$$\alpha = \sqrt{\frac{\sum_{i=1}^{i=m} (d_m - \bar{d})}{m}} \quad (28)$$

where $\bar{d}$ is the mean of vector **D**. For the case studied in this article, m is equal to 16.

Experiments and localization results

Three experiments were conducted to validate the proposed localization methodology. In experiment 1, composite plates with a $(0°/90°/0°)_s$ layup were fabricated in-house. Plain weave fiber fabrics were used as the fiber system to simulate composites with quasi-isotropic material properties. In experiment 2, composite plates with $((0°/90°/0°)_{pw}/90°_{uni}/(0°/90°/0°)_{pw})$ layup were fabricated. Both plain weave fiber fabrics and unidirectional fiber fabrics were used to obtain the orthotropic material properties. In experiment 3, stiffened composite panels with two stiffeners were fabricated using $(0°/90°/0°)_s$ layup. Plain weave fiber fabrics were used as the fiber system. A two-part epoxy, FS-A23 (resin) and FS-B412 (hardener) from Epoxy System Inc., was used as the matrix system for all composite coupons. Delaminations were seeded in the composite plates and panels during fabrication using Teflon patches. Flash thermography (EchoTherm System) was used to validate the position and size of the delaminations. The composite plates and stiffened panels with flash thermography images are shown in Figure 20.

A PZT array using eight PZT transducers was bonded on the surface of the composite samples in four pairs, as shown in Figure 20. In each PZT pair, the two transducers were placed close to each other. One PZT was used as the actuator, and the other three PZT pairs were used as sensors. In order to optimize the central frequency of the actuation signal, several actuation signals were generated using central frequencies varying from 10 to 300 kHz in 10-kHz increments. A 4.5-cycle cosine windowed burst signal with a central frequency of 180 kHz was chosen as the actuation signal. Ten observations were recorded at each measurement, and the sensor signal was averaged from these observations to reduce the sampling error. Round robin tests were conducted to improve the localization accuracy.

In experiment 1, the composite plate with quasi-isotropic material properties was tested. Baseline data were collected from the healthy composite sample. GW sensor data were collected from the sample with seeded delamination. The Lamb wave signals were analyzed using the MPD algorithm. The Lamb wave modes recorded from both the healthy sample and the sample with seeded delamination were represented in the time–frequency domain. By comparing the two TFRs in the time–frequency domain, the first converted mode caused by the delamination can be identified, as shown in Figure 21. From the TFRs of the master sensor and the nearby slave sensor, the difference of the ToF of the converted mode can be calculated, as shown in Figure 21.

The delamination localization results are shown in Figure 22. The real delamination position is 10.2 mm away from the estimated delamination position but still in the 95% confidence range of the estimated

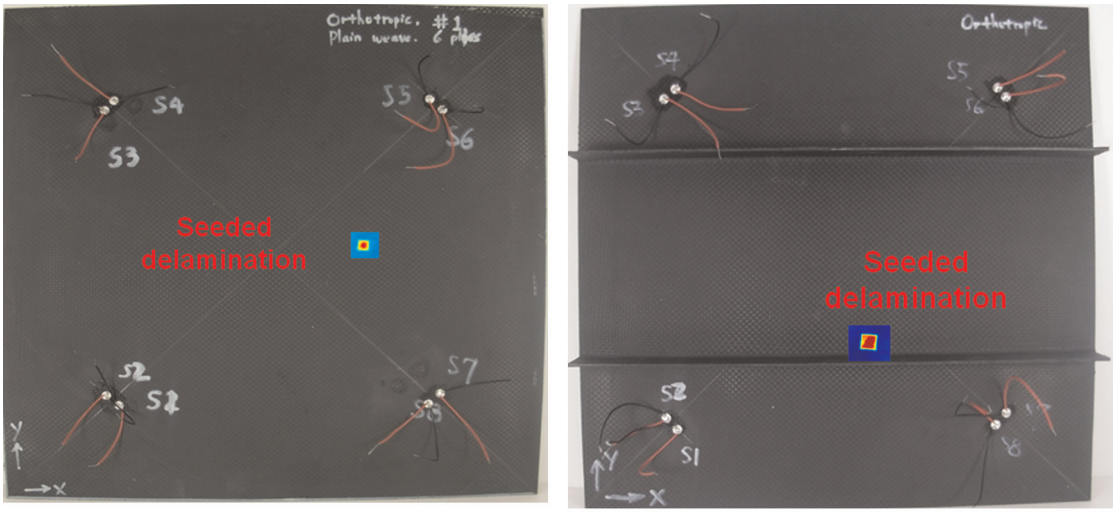

Figure 20. Composite plates and stiffened panels used in experiments.

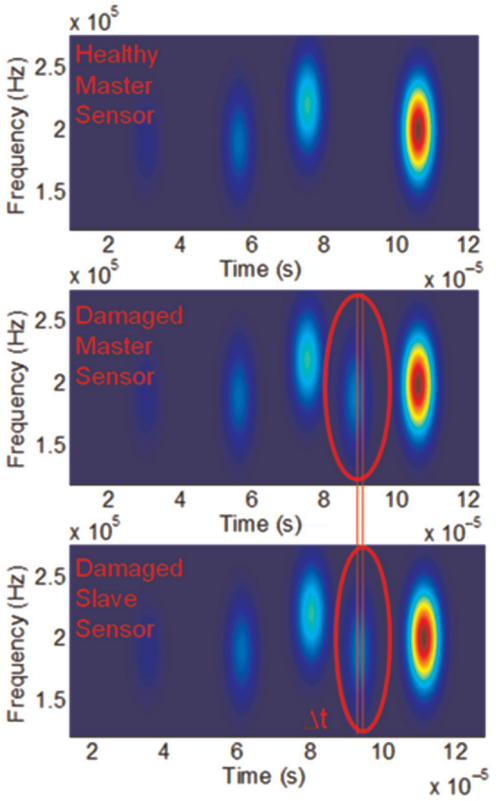

Figure 21. TFRs of the Lamb wave signals collected from master sensor in healthy plate, master, and slave sensors from damaged plate.

delamination area. The detailed real and estimated delamination positions are shown in Table 4.

Experiment 2 validated the proposed methodology using the composite plates with the orthotropic material properties. Both plain weave and unidirectional fiber fabrics were used. The ToF difference between PZT sensors was computed using the MPD algorithm. The delamination localization results show that the real delamination is 12.6 mm off the estimated delamination position, as shown in Figure 23, and the detailed real and estimated positions are shown in Table 4.

Experiment 3 validated the proposed methodology using the composite plates with two stiffeners. Similar to the approach used previously, the MPD algorithm was used to calculate the ToF difference between sensors. The delamination location was calculated by solving the optimization objective function. Localization results show that the real delamination position is 12.2 mm away from the estimated position, as shown in Figure 24. The detailed real and estimated delamination positions are shown in Table 4.

Conclusion

Time–frequency analysis–based damage detection approach using the MPD algorithm is proposed in this article. By using a small time–frequency atom dictionary, the computation cost is reduced. The propagation of Lamb waves in a stiffened carbon fiber polymer matrix composite panel is characterized. Each Lamb wave mode is accurately identified using the MPD algorithm. A two-step strategy for detection and characterization of delaminations in stiffened composite panels is developed using the proposed MPD algorithm. By identifying the converted mode caused by delaminations, the pulse-echo scheme rapidly detects the existence of delamination in the composite panel using only one PZT ring. The pitch-catch scheme detects and quantifies the delaminations in the area between the PZT actuator and sensors. A damage index based on the Lamb wave energy is proposed to quantify the

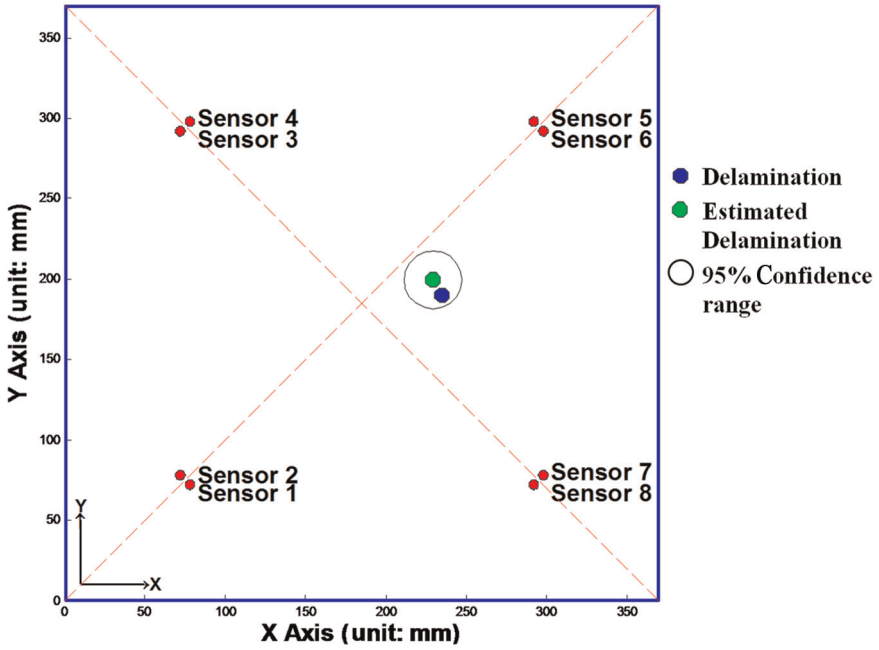

Figure 22. Estimated delamination position and confidence range for quasi-isotropic composite materials.

Table 4. Real and estimated delamination positions

	Real position (unit: mm)	Estimated position (unit: mm)	95% Confidence range (unit: mm)
Experiment 1	235.4, 190.7	229.3, 199.5	18.3
Experiment 2	240.1, 120.9	248.3, 130.5	21.5
Experiment 3	110.2, 115.6	119.3, 123.7	19.8

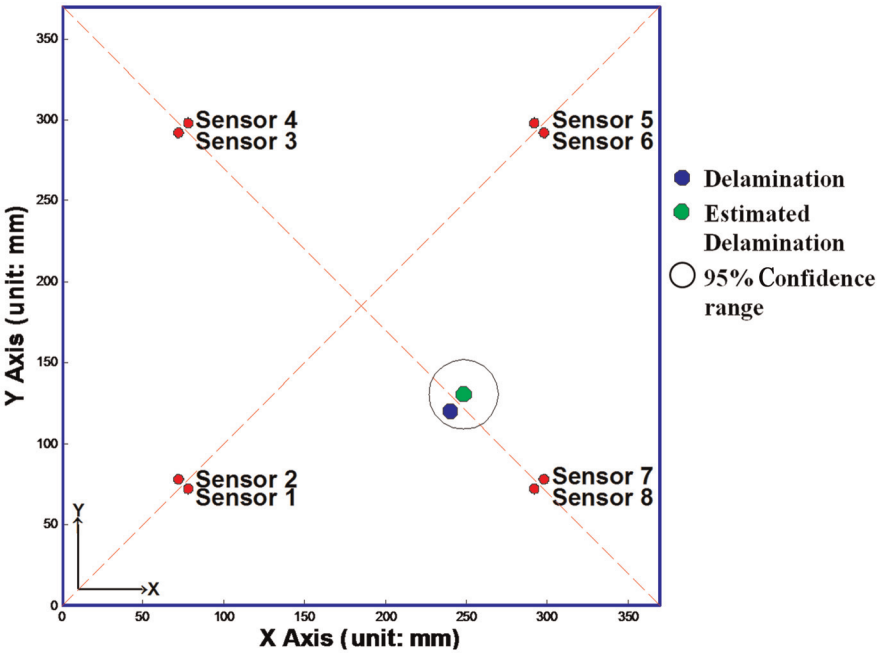

Figure 23. Estimated delamination position and confidence range for the orthotropic composite materials.

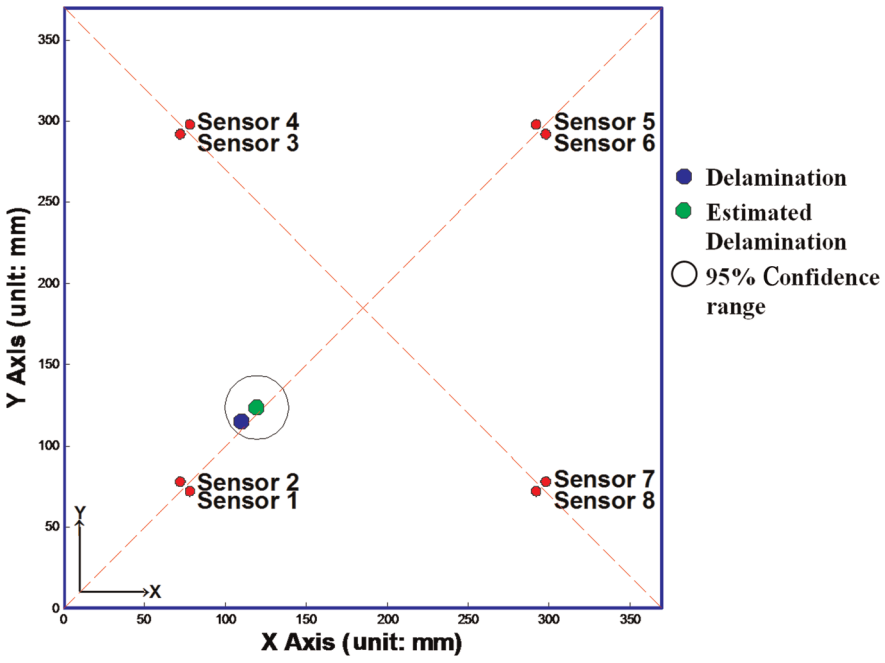

Figure 24. Estimated delamination position and confidence range for composite panels with two stiffeners.

delaminations in composite panels. Multiple damages in one composite sample can be detected.

A delamination localization methodology is further developed using the MPD algorithm. Three pairs of PZTs are used to estimate the damage position. Every two PZTs are placed next to each other. One PZT sensor is used as the master sensor, and the others are used as slave sensors. The group velocities of two nearby PZT sensors are assumed to be the same. The difference of ToF between the master and slave sensors is calculated using the MPD algorithm. By solving an optimization function subject to three nonlinear objective equations, the delamination position can be estimated without knowing the group velocity or ToF for each wave mode. Redundant sensors are placed on the surface of composite samples to estimate the 95% confidence range of the delamination position. The proposed localization methodology is experimentally validated using in-house fabricated composite plates and stiffened panels. The experimental results demonstrated that the real delamination positions can be accurately located in the 95% conference range of the estimated positions.

Acknowledgements and Funding

This material is based on research sponsored by the Army Research Laboratory and managed by the Air Force Research Laboratory/Space Vehicles Directorate under agreement number FA9453-09-1-0316. The US government is authorized to reproduce and distribute reprints for governmental purposes notwithstanding any copyright notation thereon. The views and conclusions contained herein are those of the authors and should not be interpreted as necessarily representing the official policies or endorsements, either expressed or implied, of Army Research Laboratory, Air Force Research Laboratory, or the US government.

References

Adewuyi AP and Wu ZS (2010) Modal macro-strain flexibility methods for damage localization in flexural structures using long-gage FBG sensors. *Structural Control and Health Monitoring* 18: 341–360.

Banerjee S, Ricci F, Monaco E, et al. (2007) Autonomous impact damage monitoring in a stiffened composite panel. *Journal of Intelligent Material Systems and Structures* 18: 623–633.

Chakraborty D, Kovvali N, Wei J, et al. (2009) Damage classification structural health monitoring in bolted structures using time–frequency techniques. *Journal of Intelligent Material System and Structures* 20: 1289–1305.

Coverley PT and Staszewski WJ (2003) Impact damage location in composite structures using optimized sensor triangulation procedure. *Smart Materials and Structures* 12: 795–803.

Dalton RP, Cawley P and Lowe MJS (2001) The potential of guided waves for monitoring large areas of metallic aircraft fuselage structure. *Journal of Nondestructive Evaluation* 20: 29–46.

Das S, Kyriakides I, Chattopadhyay A, et al. (2009) Monte Carlo matching pursuit decomposition method for damage quantification in composite structures. *Journal of Intelligent Material System and Structures* 20: 647–658.

Diligent O, Granhn T, Bostrom A, et al. (2002) The low frequency reflection and scattering of the S0 Lamb mode from a plate: Finite element, analytical and experimental studies. *Journal of the Acoustical Society of America* 112: 2589–2601.

Farrar CR and Lieven NAJ (2007) Damage prognosis: the future of structural health monitoring. *Philosophical Transactions of the Royal Society A* 365: 623–632.

Fasel TR and Todd MD (2010) Chaotic insonification for health monitoring of an adhesively bonded composite stiffened panel. *Mechanical Systems and Signal Processing* 24: 1420–1430.

Giurgiutiu V (2005) Tuned Lamb wave excitation and detection with piezoelectric wafer active sensors for structural health monitoring. *Journal of Intelligent Material Systems and Structures* 16: 291–305.

Hiche C, Coelho C, Chattopadhyay A (2011) A strain amplitude-based algorithm for impact localization on composite laminates. *Journal of Intelligent Material Systems and Structures*, 22(17): 2061–2067.

Ihn J-B and Chang F-K (2004a) Detection and monitoring of hidden fatigue crack growth using a built-in piezoelectric sensor/actuator network: part I. Diagnostics. *Smart Materials and Structures* 13: 609–620.

Ihn J-B and Chang F-K (2004b) Detection and monitoring of hidden fatigue crack growth using a built-in piezoelectric sensor/actuator network: part II. Validation through riveted joints and repair patches. *Smart Materials and Structures* 13: 621–630.

Kessler SS, Spearing SM and Soutis C (2002) Damage detection in composite materials using Lamb wave methods. *Smart Materials and Structures* 11: 269–278.

Kim HS, Chattopadhyay A and Ghoshal A (2003) Characterization of delamination effect on composite laminates using a new generalized layerwise approach. *Computers & Structures* 81: 1555–1566.

Kim SB and Sohn H (2007) Instantaneous reference-free crack detection based on polarization characteristics of piezoelectric materials. *Smart Materials and Structures* 16: 2375–2387.

Liu Y, Mohanty S and Chattopadhyay A (2009) A Gaussian process based prognostics framework for composite structures. In: *Processing of SPIE modeling, signal processing, and control for smart structures*, San Diego, CA, 11 March.

Liu Y, Mohanty S and Chattopadhyay A (2010) Condition based structural health monitoring and prognosis of composite structures under uniaxial and biaxial loading. *Journal of Nondestructive Evaluation* 29(3): 181–188.

Lu Y, Ye L, Wang D, et al. (2009) Time-domain analyses and correlations of Lamb wave signals for damage detection in a composite panel of multiple stiffeners. *Journal of Composite Materials* 43: 3211–3230.

Mallat S and Zhang Z (1993) Matching pursuits with time–frequency dictionaries. *IEEE Transactions on Signal Processing* 41: 3497–3415.

Meo M, Zumpano G, Pigott M, et al. (2005) Impact identification on a sandwich plate from wave propagation responses. *Composite Structures* 71: 302–306.

Mohanty S, Chattopadhyay A and Peralta P (2010) Adaptive residual useful life estimation of a structural hotspot. *Journal of Intelligent Material Systems and Structures* (special issues on SHM) 21: 321–335.

Moll J, Schulte RT, Hartmann B, et al. (2010) Multi-site damage localization in anisotropic plate-like structures using an active guided wave structural health monitoring system. *Smart Materials and Structures* 19: 04502–04517.

Papoulis A and Pillai SU (2002) *Probability, Random Variables and Stochastic Processes*. 4th ed. New York: McGraw-Hill.

Raghavan A and Cesnik CES (2007) Review of guided-wave structural health monitoring. *Shock and Vibration Digest* 39: 91–114.

Rao SS (1996) *Engineering Optimization-Theory and Practice*. New York: Wiley.

Reynolds WD, Coelho C, Kim SB, et al. (2009) Active damage localization in anisotropic materials using guided waves. In: *50th AIAA/ASME/ASCE/AHS/ASC, structures, structural dynamics, and materials conference (SDM)*, Palm Springs, CA, 4–7 May.

Salamone S, Bartoli I, Rhymer J, et al. (2011) Validation of the piezoelectric rosette technique for locating impacts in complex aerospace panels. In: *Proceeding of SPIE, smart structures and materials/NDE*, San Diego, CA, 6–10 March.

Sohn H, Park H, Law KH, et al. (2005) Instantaneous online monitoring of unmanned aerial vehicles without baseline signals. In: *Processing of 23rd international modal analysis conference*, Orlando, FL, 31 January to 3 February.

Staszewski WJ, Mahzan S and Traynor R (2009) Health monitoring of aerospace composite structures—active and passive approach. *Composite Science and Technology* 69: 1678–1685.

Su ZQ, Ye L and Lu Y (2006) Guided Lamb waves for identification of damage in composite structures: a review. *Journal of Sound and Vibration* 295: 753–780.

Wang L and Yuan FG (2006) Active damage localization technique based on energy propagation of Lamb waves. *Smart Structures and Systems* 3: 201–217.

Zhao X, Gao H, Zhang G, et al. (2007) Active health monitoring of an aircraft wing with embedded piezoelectric sensor/actuator network: I. Defect detection, localization and growth monitoring. *Smart Materials and Structures* 16: 1208–1217.